An Innovative Solar-Driven Thermo-hydraulic Ultrafiltration Process. Part I: Hydraulic Experiments and Modeling

Corentin Koninck, Driss Stitou, Moad Mahboub, Emmanuel Hernandez, Jean-Jacques Huc, Vincent Goetz

An innovative solar driven thermo-hydraulic ultrafiltration process. Part I: hydraulic experiments and modelling.

Corentin Koninck[a,b,], Driss Stitou[a], Moad Mahboub[a], Emmanuel Hernandez[b], Jean-Jacques Huc[b], Vincent Goetz[a]*

[a] PROMES CNRS, UPR 8521, Rambla de la thermodynamique 66100 Perpignan, France

[b] University of Perpignan Via Domitia, 52 Paul Alduy, 66100, Perpignan, France

*Corresponding author: corentin.koninck@promes.cnrs.fr

Keywords: Ultrafiltration, thermo-hydraulic process, energy recovery, solar energy, modelling.

Abstract:

Ultrafiltration technology is an easy-to-implement, energy efficient and selective disinfection method for a wide range of pollutants that can facilitate access to drinking water, one of the major worldwide challenges of this century. The work presented here is the first part of a study investigating an innovative thermo-hydraulic ultrafiltration process. The process is powered by solar thermal energy supplied at 40-70°C by a simple flat-plate solar collector to pump and pressurise the water to be treated by an ultrafiltration module. The preliminary experimental study carried out and presented in this paper has enabled characterisation of the hydraulic pumping/pressurisation devices with an energy efficiency ranging from 0.9 to 0.75. The backwashing device ensured a pressure ratio between the filtration and backwashing varying between 0.85 and 1.1. Series of 30-minute filtration of river water taken downstream of a wastewater treatment plant, carried out at a transmembrane pressure of 1.5 bar and followed by a 3-minute backwash, made it possible to achieve a stabilisation of the membrane permeability between 70 and 80% of its initial permeability. An unsteady-state numerical model was developed to simulate and analyse the behaviour of the process in filtration mode and during backwashing. The average deviations that were observed between simulated and experimental results amounted to 6.4% for flow rates and 1.6% for pressures.

1. Introduction

Access to clean water is still a major problem for 2 billion people worldwide. The consumption of unsafe water can lead to serious health complications (cholera, diarrhea, dysentery, etc.) and even death in some cases, mainly among the elderly and young children. More than 800,000 people die every year due to a lack of access to water, sanitation, or hygiene [1]. This issue is generally associated with deficient sewage, wastewater systems and energy distribution networks, particularly in developing countries and their rural areas. In many developing countries, rural populations are the most exposed to the use of water that is unfit for consumption, where the main health threat lies in the presence of pathogenic micro-organisms [2]. The economic challenge of connecting water and electricity in these isolated areas requires the development of decentralised water treatment and disinfection systems to meet the needs of many small, remote communities [3].

Among existing disinfection technologies, membrane filtration, which has been developing for several decades [4], is easy to use, energy-efficient and selective for a wide range of pollutants. Membrane filtration removes particles or contaminants from water by preventing them from passing through a porous medium. Two distinct liquid flows are obtained at the outlet of a membrane filtration operation: one concentrated in contaminants (the concentrate) and the other filtered (the permeate). The size of contaminants that can be separated during filtration depends on the porosity of the membrane. Different types of membranes can be used depending on the intended water treatment: microfiltration (MF), ultrafiltration (UF), nanofiltration (NF), or reverse osmosis (RO). Although NF and RO membranes have a significant capacity for retaining microorganisms, high operating pressures are required for the water to be treated, making their use uneconomical for disinfection applications aiming at eliminating pathogenic microorganisms [5]. In contrast, the pore diameter of an ultrafiltration (UF) membrane is small enough to ensure the retention of even the smallest microorganisms such as viruses and requires lower operating pressures [6]. For some years now, ultrafiltration combined with preliminary pretreatment has been considered to be a reliable solution for replacing all or part of conventional treatments (coagulation, flocculation, sedimentation, sand filtration). Ultrafiltration therefore efficiently provides biologically stable treated water, while significantly reducing the use of consumable

chemicals, such as chlorine [7]. Microfiltration (MF), on the other hand, is not selective for viruses but can be an effective treatment for removing bacteria or can be used as a pre-treatment for UF or NF [8]. In the case of clarification or disinfection processes, ultrafiltration is generally performed in semi-dead-end mode, where dead-end filtration cycles without concentrate (or retentate) production, are alternated with membrane cleaning cycles. One of the most common methods used to clean membrane surfaces is backwashing. This involves forcing a flow of clean water (often permeate) in the opposite direction to the permeation flow. This action helps to unclog the membrane from a buildup of impurities accumulated on its surface, reducing membrane permeability and filtration performance. As with filtration, the clean water must also be pressurised to remove these particles, generally with a backwash pressure of the same order of magnitude or higher than the filtration pressure [9]. This disinfection technique has been developed thanks to hollow-fiber membranes, making it cost-effective to implement [10]. The energy efficiency of such membrane processes is commonly discussed in terms of electrical energy consumed by pressurisation pumps to produce 1 cubic meter of permeate. For large scale installations, this generally ranges from 0.1 to 0.35 $kWh_{elec}.m^{-3}$. This order of magnitude is similar to the one obtained with conventional water treatment processes [10 – 11].

The pressure required to pass water through the UF membrane can be of low intensity (a few meters of water column height) and can thus be provided by manual pumping action or gravity but with the result of a low filtration flow rate. According to the study by Pronk et al. [12], an UF membrane module powered by the hydrostatic pressure of 1 meter of water column height (around 0.1 bar), can produce a stable high-quality permeate flow of around 5 $L.h^{-1}$ per m^2 of membrane from surface water. In partnership with several non-governmental organisations, Fonto de Vivo company has developed an UF system certified by the World Health Organisation (WHO), which operates with a manual pump [13]. In the same vein, Arnal et al. have also developed an UF device capable of producing 1000 $L.day^{-1}$, in which the water is pumped and pressurised to a maximum pressure of 3 bar by a pump operated manually by means of a steering wheel [14].

To avoid the need for human action and obtain higher permeate production in the case of remote areas not connected to the electrical network, it is necessary to use other energy resources to pressurise the water. With this objective, solar energy offers several advantages, such as (i) the fact that its availability and demand for clean water are perfectly matched [15], (ii) its sustainable

nature, and (iii) the low investment cost of solar equipment [16]. While many studies have been carried out on nanofiltration or reverse osmosis processes for solar desalination using photovoltaic (PV) panels, there are only a few studies in the literature on solar ultrafiltration processes for drinking water production [17]. Rainwater ultrafiltration has been studied numerically in Cambodia [18] and experimentally in Brazil [19]. High permeate flow rates (135 $L.h^{-1}.m^{-2}$) were obtained with filtered water quality in line with WHO standards, assuming sufficient rainfall. However, the authors mention that one of the main difficulties lies in the mismatch between solar energy availability and rainwater treatment. It is therefore mandatory to install in such systems large water storage or batteries. Solar-driven ultrafiltration of surface water has also been studied by Chew and David Ng [20], who developed a UF filtration system equipped with a 4.0 m^2 membrane, a pump, and a 50 W PV panel coupled to a battery. Filtration was performed tangentially in order to limit fouling problems, the number of backwashes and the associated treated water losses. This prototype, designed to meet the water needs of a village in Malaysia, successfully treated river water with a specific electrical consumption of 0.18 $kWh_{elec}.m^{-3}$ of drinking water produced. These performances are comparable to those reported in the literature review conducted by Davey and Schäfer [17], regarding the specific energy consumption obtained for various ultrafiltration systems, which range from 0.1 to 0.35 $kWh_{elec}.m^{-3}$. Taking into account the overall conversion efficiency of solar energy into electricity of the photovoltaic panels (η_{PV}), which currently varies from 0.1 to 0.2 depending on the cell technology used [21-22], specific solar energy consumed by these processes can then be defined in relation to the incident solar resource. Photovoltaic membrane ultrafiltration processes can thus be characterised by an overall specific solar energy consumption ranging from 0.5 to 3.5 $kWh_{sol}.m^{-3}$ of potable water produced.

This study focuses on a new solar ultrafiltration process that also uses solar energy but in thermal form. In such a thermo-hydraulic process, the water is pumped and pressurised by a hydraulic cylinder driven by an Organic Rankine Cycle engine (ORC) powered by low-grade heat supplied at 40 - 70°C by flat plate solar collectors. The study aims to (i) propose an innovative configuration of water treatment process by ultrafiltration operating by means of solar thermal collectors, (ii) demonstrate the technical feasibility of such an ultrafiltration process powered by low-temperature thermal energy, (iii) evaluate its energy performance and compare it to conventional or solar UF processes, and (iv) analyse the impact of solar intermittence on the quantity and quality of drinking water produced. In this first part, the study focuses solely and preliminarily on the hydraulic

operation of the process. It is driven by compressed air, in order to emulate the pressures of evaporation and condensation obtained in the ORC. In this way, aspects linked to the conversion of solar energy into heat by the solar collector and then into pressure energy by the ORC cycle are set aside. The objective is to focus on the characterisation and the behaviour analysis of the main hydraulic components of such a thermally-driven UF process. This preliminary phase is important to ensure that the major components are working properly. To this end, a numerical model is developed and compared with the results of experiments carried out under controlled pressure conditions. A backwash device is also investigated using numerical and experimental approaches to define an effective cleaning protocol for the UF membrane.

2. The innovative thermo-hydraulic process for membrane filtration

In conventional membrane filtration processes, water is supplied by pumps powered by the electricity grid or photovoltaic panels in isolated areas. The innovative feature of the thermo-hydraulic water treatment process presented in this article and schematically described in Figure 1, lies in the exploitation of thermal energy instead of electricity to pump and pressurise the water to be treated. The thermal energy can be either waste heat, which can be recovered, or supplied by flat-plate solar collectors, extremely robust and reliable components. This innovative process is an adapted evolution of the thermo-hydraulic process developed by Lacroix et al. [23] at the PROMES-CNRS laboratory and specifically designed for desalination of brackish water by reverse osmosis.

2.1. Presentation of the complete solar thermo-hydraulic process

This new variant consists of four main interconnected parts. The first part is dedicated to collecting and converting solar energy into thermal energy to power a Rankine thermodynamic engine cycle (ORC). The collected thermal energy is supplied to heat and evaporate at high pressure the working fluid (n-butane) of the ORC cycle. The range of saturated pressure-temperature equilibrium that can be achieved with n-butane corresponds well to the usual operating temperature of a solar collector and filtration pressure of the UF module. The wide geographical availability of such a working fluid is also a significant advantage. The high pressure vapour produced in the evaporator allows it to directly pressurise a volume of water contained in a bladder-type hydropneumatic tank,

which forms the second part of the system. The role of this second block is to transmit the work produced by the ORC cycle to a third part of the device, consisting of a double-acting hydraulic cylinder with 2 chambers, which, on the one hand, pumps the water to be treated and, on the other hand, pressurises this water to be filtered. The water to be treated pumped in this way is also used as a cold source of the ORC in order to condense the working fluid vapour.

Thanks to this design, the hydraulic actuator, which is driven by the transfer liquid pressurised in a first bladder reservoir by the evaporator, simultaneously (i) pumps the water to be treated, (ii) pressurises the transfer liquid that fills the second bladder tank to a suitable pressure so that this liquid can discharge the ORC cycle working fluid contained in the bladder to the condenser, and (iii) supplies the membrane with pressurised water to be treated. Finally, the last block is the ultrafiltration module, which operates in a dead-end mode to produce permeate. The water to be treated which is pumped by the double-acting cylinder, is also used as a coolant for the condenser to condense the working fluid of the ORC engine cycle drawn from the bladder tanks.

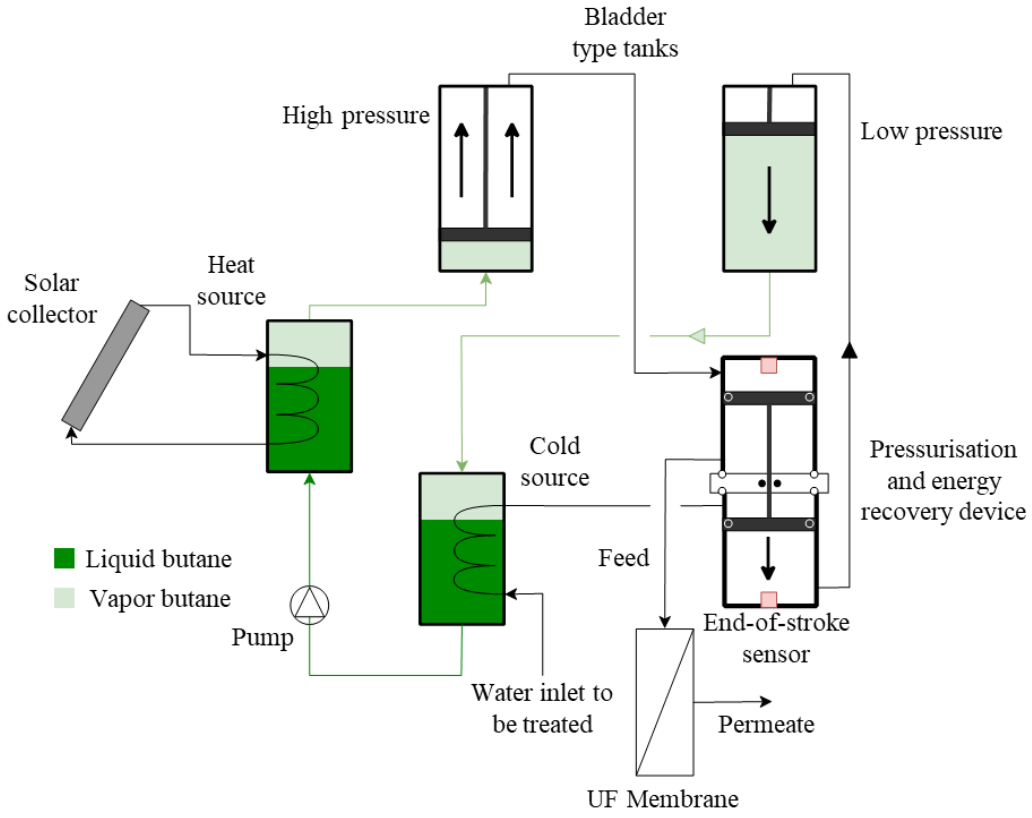

Figure 1. Schematic block diagram of the whole solar thermal membrane filtration process

When the hydraulic cylinder's end-of-stroke is reached, a set of solenoid valves and non-return valves, not shown in this figure, make it possible to switch the operating phases by reversing the role of the two bladder tanks for continuous operation. Finally, a liquid pump achieves the transfer of the ORC working fluid (n-butane) from the condenser to the evaporator.

In this preliminary feasibility study of this innovative process, only the last three main components representing the hydraulic part specifically related to water treatment are studied. The driving part, consisting of the solar collector and the ORC engine cycle, generating the high (HP) and low (LP) operating pressures of the process, is replaced by a compressed air supply device. The feed of the HP bladder tank is controlled by a pressure reduction regulator, while the discharge of the LP bladder tank is controlled by an open-air back-pressure regulator. In this way, the operating pressures of the HP and LP bladder tanks simulate thus the saturation vapour pressures of the working fluid (n-butane) in the evaporator and the condenser of the ORC cycle, according to their operating temperatures. For the low pressure condenser, condensation will be achieved by using pumped water to be treated at ambient temperature, varying between 10 to 40°C depending on seasonality and location. The resulting condensing pressures will range therefore from 1.5 to 4 bar All pressures given in this study are absolute pressures. Evaporator operation at high-pressure will directly be dependent on the operating temperature of a conventional flat solar collector, which typically delivers heat between 40 and 70°C. These operating temperatures imply an evaporator operating pressure of between 4 and 10 bar. In addition, a sufficient difference between evaporating and condensing pressure i.e. HP and LP must be taken into account in order to generate an acceptable driving pressure difference in the hydraulic double-acting cylinder to enable it to move.

2.2. Description of the hydraulic parts of the UF process

Figure 2 details the hydraulic part of the UF filtration process operated with compressed air. Circuits in bold represent the portions of the hydraulic system under high pressure, which is imposed by the set pressure of the pressure-reducing regulator. The pressure transmission part between the compressed air and the water to be treated consists of two bladder-type tanks, one of which feeds the double-acting cylinder with HP transfer liquid, which in turn fills the second one with transfer liquid (water) at a low-pressure controlled by the back-pressure regulator. The sealing between the compressed air and the liquid transfer in the bladder-type reservoir is achieved by a

nitrile long-stroke rolling diaphragm (from SIMRIT manufacturer) whose deformation is guided by a sliding shaft. The complete amplitude of movement of the diaphragm corresponds to a displaced volume of transfer liquid (water) equal to 2.7 L. The liquid transfer (water) contained in the upper part of each bladder tank is kept under pressure by the air, the pressure of which is either controlled by the pressure reducing regulator of the backpressure regulator. A set of two 3-way solenoid valves alternately connects one of the bladder tanks to compressed air while the second is connected to the air exhaust. When one of the tanks, pressurised by the compressed air, discharges water under pressure to the hydraulic actuator, the second one, connected to the air exhaust, is maintained at a low pressure fixed by the back-pressure regulator and fills up with water by the displacement of the hydraulic actuator.

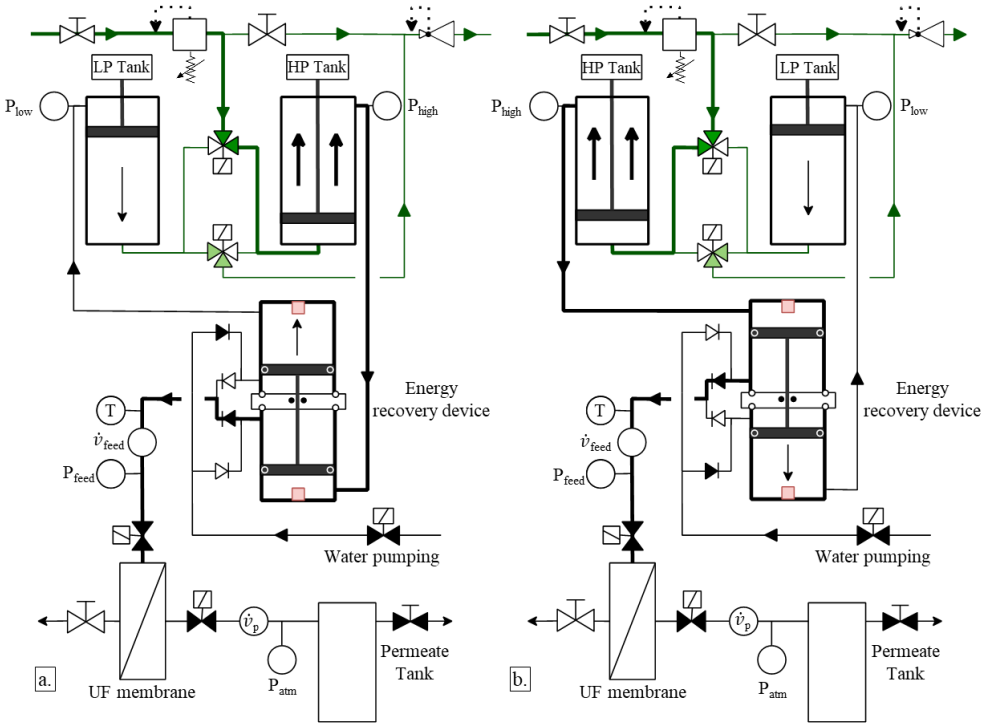

Figure 2. Schematic diagram of the hydraulic part of the membrane filtration process in (a) phase I and (b) phase II. The green lines (—) represent compressed air piping and the black lines (—) indicate the piping of the transfer liquid (water) and the water to be treated, the red square (□) symbolises the end-of-stroke sensor.

This alternating filling and emptying of the tanks is controlled by the double-acting hydraulic cylinder, which also pumps and pressurises the water to be treated. This double-acting cylinder is

equipped with two end-of-stroke switches located at its ends, which simultaneously activate or deactivate the two 3-way solenoid air valves, thus ensuring the transition between phase I (Fig. 2a) and phase II (Fig. 2b), and vice versa, by reversing the role of the bladder tanks. The two chambers of the hydraulic cylinder are designed with a displacement volume of 2.6 L, which is slightly lower than the volume of water cycled in the bladder tanks. In this way, the hydraulic actuator always reaches its ends and does not stop due to a lack of pressurised water. The hydraulic cylinder is, therefore, the only hydraulic device that controls the cyclic operating of the UF process by actuating the alternative connections of the bladder tanks to either the high-pressure air supply (simulating the evaporator) or the low-pressure exhaust air (simulating the condenser).

Thus, thanks to the hydraulic energy from the pressurised bladder tank, the double-acting cylinder also makes it possible, by means of its internal chamber, to pressurise the water to be filtered at the supply pressure (P_{feed}) that is appropriate for the membrane module and to pump the water to be treated. These two actions are carried out passively and simultaneously thanks to the set of four non-return valves that allow the water to be treated to draw in and pressurise water to be supplied to the UF module.

The entire process was controlled and managed by a LabVIEW program thanks to the digital input signals provided by the end-of-stroke switches of the double-acting cylinder. When one of these switches is activated, a signal is sent to the program, which in return changes the position of the two 3-way solenoid valves of compressed air, so that the operating phase of the process can be reversed. The activation of the 2-way solenoid valves ensures the flow circulation of the water in the process and to the membrane module.

The membrane module (UF20 M2, Polymem), composed of polysulfone hollow fibres with a pore size of 10 nm, is characterised by the manufacturer as having a total filtration area of 0.38 m^2 and a pure water permeability L_0 = 70 $L.h^{-1}.m^{-2}.bar^{-1}$ at 20°C. Although it is possible to perform filtration in a cross-flow mode, the dead-end mode was chosen for the experiments, in order to limit hydraulic and energy losses linked by concentrate recirculation. To comply with the mechanical constraints acceptable by the membrane, the transmembrane pressure (TMP) was limited to a maximum value of 2.5 bar. The permeate produced is then stored in a dedicated reservoir. The characteristics of the main hydraulic components and data acquisition sensors are

summarised in Tables S1 and S2 in part S1 of the supporting information section. Their location on the experimental bench is shown in Figure 3.

The pressures, flow rate, and temperature of the water to be treated are measured at the inlet and outlet of the hydraulic cylinder thanks to pressure sensors, flowmeters and thermocouples. Experimental data are recorded with a 2-second acquisition time step. Figure S1 (Sup. Inf. Part S2) shows the human/machine operator interface for the experimental implementation of the membrane filtration process.

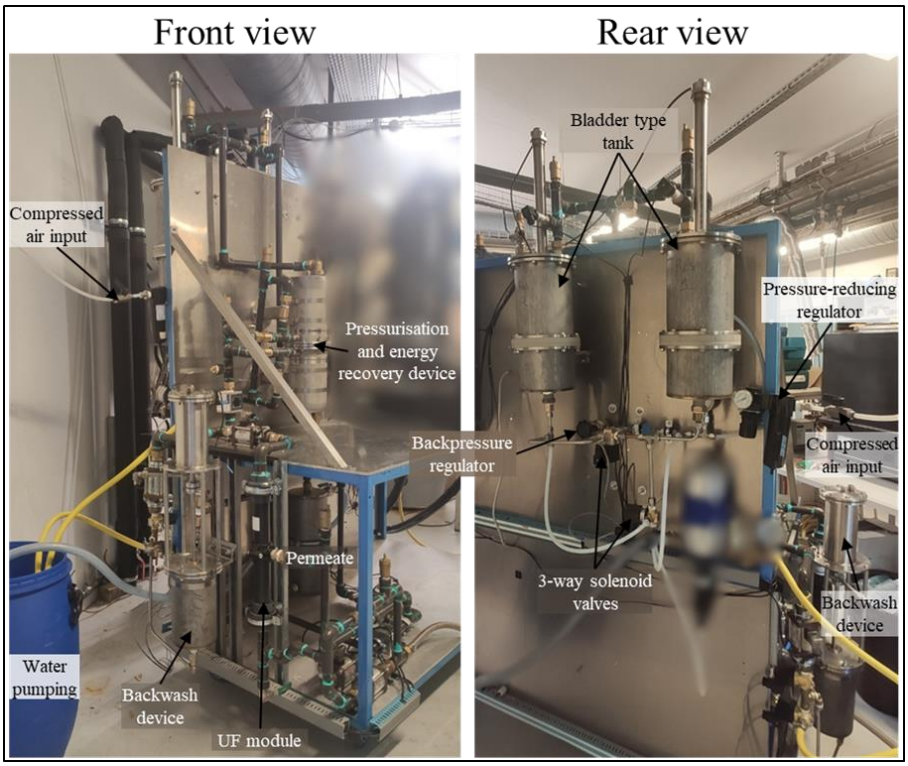

Figure 3. Rear and front views of the experimental bench of the compressed air-driven membrane filtration process

A preliminary series of experiments was carried out on this hydraulic system in order to characterise the different components of the device, and more specifically the hydraulic cylinder and the UF membrane. The low (P_{low}) and high (P_{high}) pressures were respectively maintained constant within a range of 1.5 to 4 bar for the discharge pressure and 4 to 7 bar for the air supply pressure with a minimum pressure difference of 1.5 bar between the two reservoirs. These pressure

operating conditions guarantee that, due to the design of the cylinder, the transmembrane pressure (TPM) does not exceed the maximum permissible value of 2.5 bar for the membrane.

3. Experimental characterisation of the main components of the UF process

The energy performance of such a process is related to the effectiveness of the pressurisation device and the recovery of the hydraulic work via the double-acting hydraulic cylinder, as well as to the filtration capacity of the module. It is therefore of key importance to first characterise the losses associated with the piston friction of the hydraulic actuator and to determine the actual permeability of the UF membrane.

3.1. Characterisations of the main hydraulic cylinder and the UF filtration module

The efficiency of the hydraulic cylinder η_{VP} can be determined by the equation from E.1 to E.3, which considers a balance between forces resisting piston movement and the forces driving the piston. These forces are determined from the piston and shaft sections, as well as the different pressures applied in the different chambers of the cylinder, including the atmospheric pressure at which the water to be treated is pumped (Fig. 4).

$$F_{resist} = \eta_{VP}.F_{dri} \quad \text{(E.1)}$$

$$S_V.P_{low} + (S_V - S_s).P_{feed} = \eta_{VP}.\left[S_V.P_{high} + (S_V - S_s).P_{atm}\right] \quad \text{(E.2)}$$

Then the efficiency of the hydraulic cylinder is expressed as:

$$\eta_{VP} = \frac{S_V.P_{low}+(S_V-S_s)P_{feed}}{S_V.P_{high}+(S_V-S_s)P_{atm}} \quad \text{(E.3)}$$

With F_{resist} [N] the resistive forces and F_{dri} [N] the driving forces applied to the piston of the cylinder, η_{VP} [-] the hydraulic efficiency of the main cylinder, $S_V = 14.9.10^{-3}$ [m^2] the internal cross-section of the cylinder chambers, $S_s = 15.4.10^{-5}$ [m^2] the cross-section of piston shaft, P_{high} [Pa] the high pressure (HP) set by the pressure-reducing regulator and P_{low} [Pa] the low pressure (LP) controlled by the backpressure regulator, P_{feed} [Pa] the resultant feed pressure to the membrane module UF and $P_{atm} = 101325$ [Pa] the atmospheric pressure at which the water to be treated is pumped.

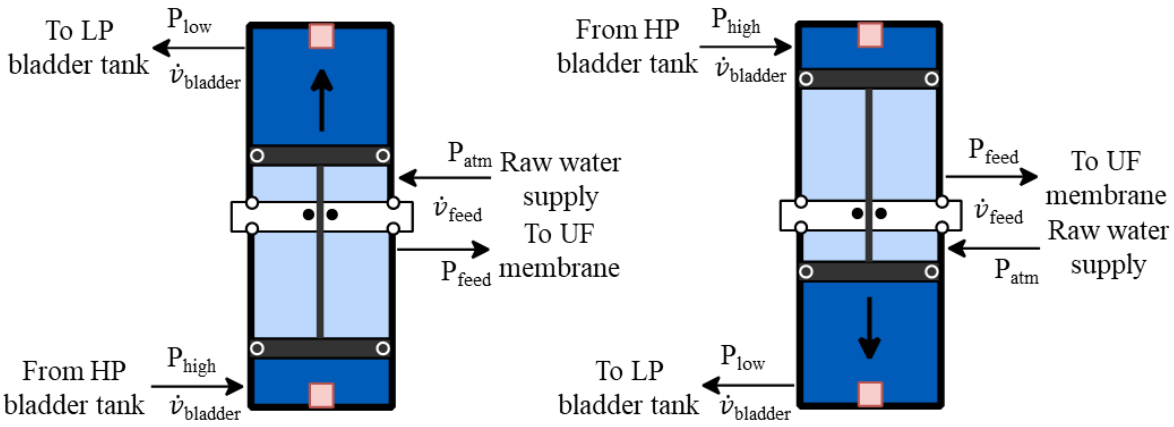

Figure 4. Schematic diagram centred on double-acting cylinder operation during the two successive phases.

The friction generated by the piston movement was relatively low in the range of operating pressures studied. Indeed, the efficiencies obtained experimentally for the cylinder, as shown in Figure 5, range from 0.86 to 0.92, with an average value of 0.89. The cylinder was specially designed and manufactured for this project in the PROMES laboratory workshop, with geometric machining uncertainties on cylinder diameters of around 10 µm to obtain a low roughness and limit friction. In addition, the measurement uncertainty of pressure sensors (0 - 10 bar, class 0.5) was around 0.05 bar. Finally, based on the experiments carried out, the hydraulic efficiency of the cylinder η_{VP} can be expressed as a function of the transmembrane pressure $TMP = P_{feed} - P_{atm}$ [Pa], using the empirical correlation (E.4).

$$\eta_{VP} = 2.7.10^{-7}.TMP + 0.858 \qquad \text{(E.4)}$$

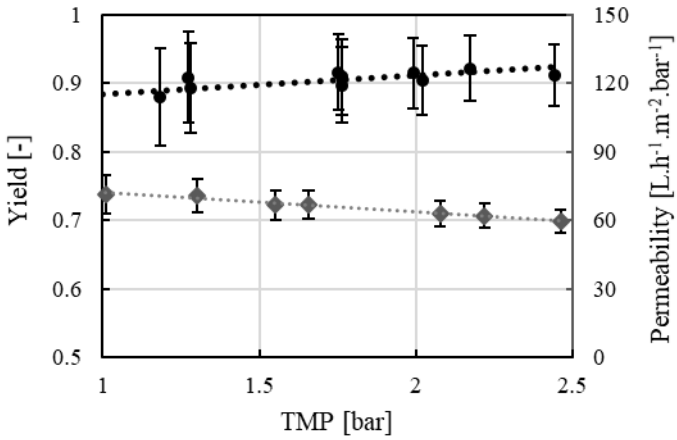

Figure 5. Experimental characterisations of the pressurisation device (●), the UF membrane (♦) and their associated correlation (dotted lines).

3.2. Characterisation of the UF filtration module

Similarly, the permeability of the membrane measured using water at 20°C from the laboratory's water distribution network and applying different transmembrane pressures was almost constant, varying between 70 and 60 $L.h^{-1}.m^{-2}.bar^{-1}$. These values were consistent with that stated by the manufacturer. This characterisation also took into account the measurement uncertainties of flowmeters and pressure sensors.

The slight decrease in permeability can be partially explained by the increasing pressure losses generated by the pipes, elbows and non-return valves placed at the inlet and outlet of the membrane module, which have not been considered. It can also be explained by an increase in hydraulic resistance R_m [m^{-1}], which is proportional to the increase in transmembrane pressure as shown by Huisman et al. and Tarnawski and Jelen [24 – 25]. To take into account this variation, the permeability L [$L.h^{-1}.m^{-2}.bar^{-1}$] of the UF module implemented was finally characterised according to the following empirical correlation as a function of the transmembrane pressure [Pa] (E.5).

$$L = - 8.447.10^{-5}.TMP + 80.5 \quad \text{(E.5)}$$

3.3. Experimental membrane filtration results

Various experiments were then carried out to analyse the behaviour of the process and evaluate its performance over the operational range of transmembrane pressure studied [1 – 2.5] bar. Four experiments were chosen to allow a representative overview of the process behaviour and

performance over the entire operating range tested. They are shown in Figure 6. The first two case studies (P_{low} = 4 bar; P_{high} = 6 bar) and (P_{low} = 4 bar; P_{high} = 6.8 bar) simulate the operation of the process with n-butane as the working fluid and in the case of high condensation temperatures, of the order of 40°C (4 bar), representative of summer operating conditions or a hot climate (Sub-Saharan Africa) (Fig. 6a and 6b). The other two cases, Fig. 6c and Fig. 6d, represent more temperate conditions for which the condensation temperature was around 30°C (3 bar) or 20°C (2 bar).

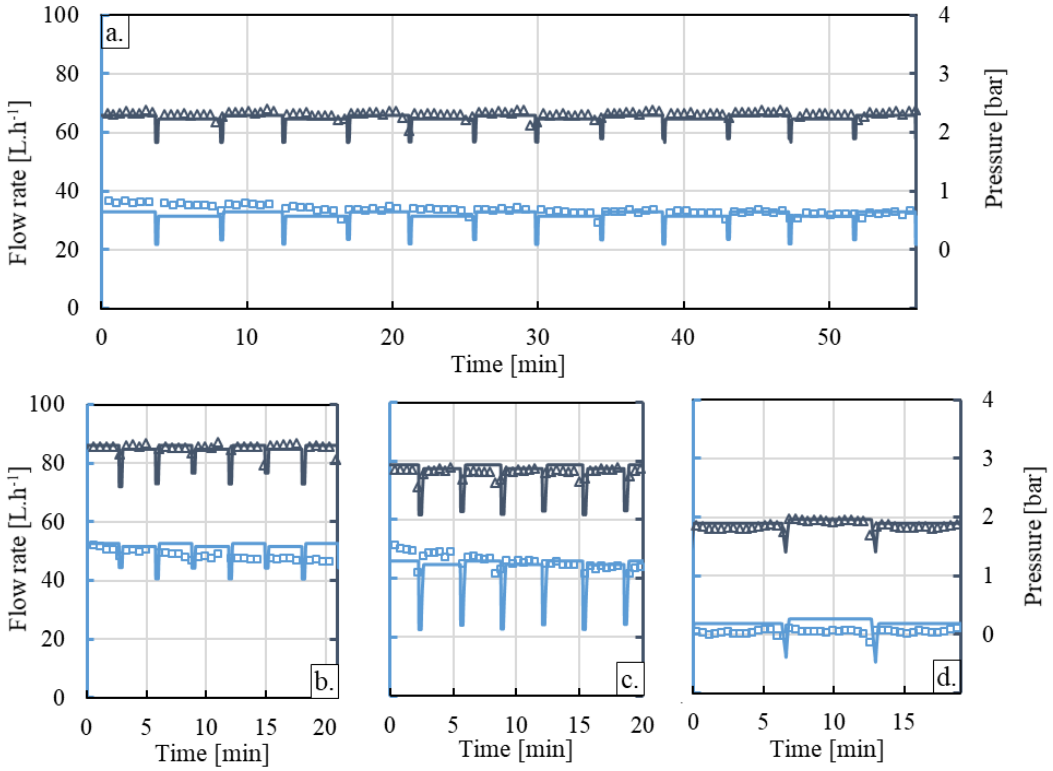

Figure 6. Simulated (continuous lines) and experimental (dots) permeate flows (□) and membrane feed pressures (Δ) obtained with clean water for 4 operating conditions : (a) P_{high} = 6 bar, P_{low} = 4 bar and TMP = 1.2 bar; (b) 6.8 bar, 4 bar and 2.1 bar; (c) 5.4 bar, 3 bar and 1.7 bar; (d) 3.5 bar, 2.1 bar and 0.9 bar.

Figure 6a shows the evolution of feed pressure to the UF module and permeate flow rate, obtained when the pressure-reducing regulator and the backpressure regulator were set at 6 and 4 bar respectively. The graphs show sharp variations in pressure and flow rate that occur cyclically. These correspond to the reversal of the movement direction of the hydraulic cylinder piston. When the piston of the hydraulic cylinder reached one end of its stroke, the corresponding switching

sensor actuated then the 3-way solenoid valves to change the direction of the displacement of the piston. For a short time, the piston was then stopped, inducing a sudden drop in the water supply pressure to the membrane module. Each time the movement of the piston was reversed, there was also a slight delay (around 5 seconds), which corresponds to the time needed to depressurise the bladder tank previously filled with high-pressure air, while pressurisation of the second tank filled with water was almost instantaneous. One complete cycle corresponds to one return stroke of the cylinder piston.

In Fig. 6a, 6.5 cycles are shown over a total operating duration of 58 minutes, i.e. an average of almost one cycle every 9 minutes. The duration of these cycles depended on the permeate flow produced by the membrane module operating in dead-end mode with the imposed transmembrane pressure. Since the volume of the cylinder chambers was 2.7 L, the permeate flow obtained was 33 $L.h^{-1}$ on average for a membrane feed pressure of 2.29 bar. The permeate pressure at the membrane outlet (not shown in the figure) was stable at 1.07 bar, giving thus a TMP of 1.22 bar. The resulting membrane permeability was 71 $L.h^{-1}.m^{-2}.bar^{-1}$, in agreement with the experimental characterisation (E.5).

For the second experiment (Figure 6b), the high pressure was increased to 6.8 bar, which resulted in an increase in the membrane feed pressure to 3.2 bar and thus that of the transmembrane pressure to 2.1 bar. The flow rate of permeate produced then increased to an average of 47 $L.h^{-1}$. The round-trip frequency of the hydraulic cylinder was faster, with a shorter cycle time of around 5.9 minutes. The third and fourth experiments were carried out respectively with a lower discharging pressure of the low-pressure tank controlled by the backpressure regulator, at 3 and 2.1 bar. The high pressure was adjusted to 5.4 and 3.5 bar to generate a membrane module feed pressure of 2.8 and 2 bar respectively. The permeate flows thus obtained were 44 $L.h^{-1}$ and 20.6 $L.h^{-1}$, inducing a similar average permeability for these two experiments around 67.9 $L.h^{-1}.m^{-2}.bar^{-1}$, in agreement again with Figure 5. In the supporting information section, Table S3 summarises the experimental results obtained for these four operating conditions.

The analysis of the graphs in Fig. 6 also showed a slight asymmetry in the feed pressure of the membrane module, depending on the direction of the movement of the cylinder piston. As shown in Fig. 6d, a difference in the UF module feed pressure around 0.1 bar can be noticed for two successive half-cycles. This difference can be explained by the vertical position of the hydraulic

cylinder, which induces an additional force related to the weight of the piston and the volume of water above it. This additional force acted as a driving force when the piston moved downwards and as a resisting force when the piston was moving upwards.

4. Numerical model of hydraulic operation for membrane filtration

To improve the overall understanding of the system, a numerical model was then developed to simulate the process behaviour and determine the water flow rates and operating pressures of this innovative hydraulic membrane filtration process.

4.1. Assumptions and presentation of equations

To develop a simplified dynamic model of the hydraulic membrane filtration process, several hypotheses were considered. These assumptions are considered to simplify the dynamic modelling of the system since their impact on the system's performance is negligible, whatever the conditions of operation.

- Bladder tanks were assumed to behave (i) identically and symmetrically; it also considered that (ii) bladders are perfectly deformable without any elastic stress, and (iii) the air inside is isothermal.
- The cylinder piston was considered to be non-deformable and behave symmetrically.
- The impact of temperature on membrane permeability is neglected, as water temperature is considered constant and equal to 20°C.
- Singular (in elbows, flowmeters, solenoid valves) and regular (in tubes) pressure losses are considered negligible, given the low flow rates in the process.

Simulation of the hydraulic process requires prior knowledge of the operating conditions, which are the ambient temperature T [K], the high pressure of the compressed air circuit P_{airHP} [Pa], the high pressure set by the P_{high} pressure-reducing regulator [Pa] and the low pressure set by the P_{low} backpressure regulator [Pa].

The pressure inside the bladder tanks imposed by the air, whether high or low, is determined by a mass balance and by considering air as a perfect gas:

- for the HP tank fed by the pressure-reducing regulator (E.6):

$$\frac{dN_{resHP}}{dt} = \frac{V_{resHP}}{RT}\frac{dP_{high}}{dt} + \frac{P_{high}}{RT}\frac{dV_{resHP}}{dt} = \dot{n}_{HP} \quad \text{(E.6)}$$

- for the BP tank controlled by the backpressure regulator (E.7):

$$\frac{dN_{resLP}}{dt} = \frac{V_{resLP}}{RT}\frac{dP_{low}}{dt} + \frac{P_{low}}{RT}\frac{dV_{resLP}}{dt} = -\dot{n}_{LP} \quad \text{(E.7)}$$

With N [mol] the number of moles, t [sec] time, V [m^3] the volume of air, P [Pa] the pressure, R = 8.314 [$J.mol^{-1}.K^{-1}$] the perfect gas constant, T = 293 [K] the ambient temperature, $\dot{n}$ [$mol.s^{-1}$] the molar flow rate, the *resHP* index denoting the high-pressure tank and the *resLP* index denoting the low-pressure tank.

Molar air flow rates are a function of the characteristics of the pressure controllers (pressure-reducing regulator or backpressure regulator), characterised by their respective flow coefficient Kv:

- for the pressure-reducing regulator:

$$\dot{n}_{HP} = 514.Kv_{resHP}\frac{\rho_{air}}{M_{m,air}}\sqrt{\frac{(P_{airHP}-P_{high}).P_{high}}{T}} \qquad \text{(E.8)}$$

- for the backpressure regulator:

$$\dot{n}_{LP} = 514.Kv_{resLP}\frac{\rho_{air}}{M_{m,air}}\sqrt{\frac{(P_{low}-P_{atm}).P_{atm}}{T}} \qquad \text{(E.9)}$$

With Kv [$Nm^3.h^{-1}$] the pressure controller flow coefficient, ρ_{air} [$kg.m^{-3}$] the air density, $M_{m,air}$ = 0.02897 [$kg.mol^{-1}$] the air molar mass and P_{airHP} [Pa] the high pressure of the compressed air circuit.

Considering a symmetrically alternating operation of the two bladder-type reservoirs whose overall volumes are 3 L each, allow a useful volume of water of 2.7 L to be cycled. When one reservoir is completely filled with water and zero air volume, the second contains a compressed air volume of 2.7 L, with a residual water volume of 0.3 L.

This symmetrical operation is guaranteed by the hydraulic cylinder, which ensures that identical volumes of water are displaced at all times of operation. The pressure difference (P_{high} - P_{low}) between the two bladder tanks enables the double-acting hydraulic cylinder to move, pumping the water to be treated at an inlet pressure P_{atm} and pressurising the feed water to the UF membrane module at P_{feed}. This latter pressure, P_{feed}, is determined from the balance of resistive and driving forces on the cylinder piston and the hydraulic efficiency of the cylinder experimentally characterised by equation E.4. The asymmetry of the cylinder operation previously observed, which is due to its vertical position and the weight action of the piston and the volume of water above it, is also considered by taking into account the upward or downward direction of displacement.

- Upward direction of piston:

$$S_V P_{low} + (S_V - S_s)P_{feed} - (M_p + M_w)g = \eta_{VP}\left[S_V P_{high} + (S_V - S_s)P_{atm}\right] \qquad \text{(E.10)}$$

- Downward direction of piston:

$$S_V P_{low} + (S_V - S_s)P_{feed} + (M_p + M_w)g = \eta_{VP}[S_V P_{high} + (S_V - S_s)P_{atm}] \quad \text{(E.11)}$$

Where M_p = 2 [kg] the mass of the cylinder piston, M_w [kg] the mass of water contained in a cylinder chamber and g = 9.81 [m.s^{-2}] the gravitational force equivalent.

The presence of the piston shaft in the inner chambers of the cylinder generates a water flow rate difference (E.12) between the flow ($\dot{v}_{bladder}$) circulating between the bladder tanks and the outer chambers of the hydraulic cylinder and that, ($\dot{v}_{feed}$), circulating between the inner chambers of the cylinder for pumping water or feeding the membrane.

$$\dot{v}_{bladder} = \frac{\dot{v}_{feed} \cdot S_V}{(S_V - S_s)} \quad \text{(E.12)}$$

With $\dot{v}_{bladder}$ [L.h^{-1}] the flow in and out of the bladder tanks, $\dot{v}_{feed}$ [L.h^{-1}] the flow in the membrane and the flow of the pumped water to be treated.

Thus, thanks to the pressure difference between the two bladder tanks, which enables the hydraulic cylinder to operate, the water to be treated is pressurised and filtered according to a dead-end mode by the membrane ultrafiltration module. The filtered water flow rate corresponds to the product of membrane permeability, membrane surface and transmembrane pressure (TMP) (E.13).

$$\dot{v}_{feed} = L.S.(P_{feed} - P_{atm}) = \dot{v}_p \quad \text{(E.13)}$$

With L [L.h^{-1}.m^{-2}.bar^{-1}] the membrane permeability given by E.5, S = 0.38 [m^2] the membrane filtration surface and $\dot{v}_p$ [L.h^{-1}] the flow of filtered water by the membrane.

The 13 equations presented (E.1 to E.13), removing the duplicate equations used to detail the cylinder efficiency calculation (E.1 to E.3) and the one used to represent the phase change (E.11), lead to a set of 9 equations with 9 unknowns. The variables calculated are the pressures within the two bladder tanks (P_{high} and P_{low}) and that upstream of the membrane P_{feed}; the molar flow rate of pressurised air incoming the high-pressure bladder tank and outgoing the low-pressure bladder tank ($\dot{n}_{HP}$ and $\dot{n}_{LP}$); the cylinder efficiency (η_{VP}); the membrane permeability (L); the flow of water circulating between the cylinder and the bladder tanks ($\dot{v}_{bladder}$) and the flow of water in and out of the membrane ($\dot{v}_{feed}$). These equations are presented in detail in part S3 of the Supporting Information section, with the associated nomenclature in part S4.

4.2. Results and Discussion

The modelling of the process thus developed made it possible to determine the evolution as a function of the time of the flow rate ($\dot{v}_{feed}$) and the operating pressure of the UF membrane module (P_{feed}). As all the time-dependant variables, they are a function of the controlled operating

parameters (pressure of compressed air supply of the network P_{airHP}, open air discharging pressure of the backpressure regulator (P_{atm}), water temperature) and the hydraulics characteristics of the various components (efficiency of the hydraulic cylinder, volumes of bladder tanks, UF module permeability, flow coefficients of the valves and pressure regulators).

Figure 6 compares the results of the simulations with those of the 4 experiments presented above. The small difference observed between experimental and simulated profiles validated the accuracy of the model developed. The cyclic experimental behaviour of the process is faithfully represented by the simulations, as evidenced by the satisfactory repeatability of the process control actuated by the end-of-stroke switches of the hydraulic cylinder.

As can be seen, a deviation is however noticeable between the simulated and experimentally produced permeate flow rates, while the simulated and experimental feed pressures P_{feed} to the membrane module, are almost coincident for all four experiments. The root-mean-square difference between the measurements and the simulated values over all cycles of these experiments was 2.06 $L.h^{-1}$ for flow rates, while it was only 42 mbar for pressures.

Similarly, as observed experimentally, the simulations also showed a slight difference in the feed pressure between two successive half-cycles, which averaged 0.06 bar over all simulations. This small deviation in pressure results from the asymmetry operating of the hydraulic cylinder operating in the vertical position: the movement of the piston is facilitated when it is moving downwards, inducing a slightly higher feed pressure than when the piston is moving upwards.

Apart from the impact of phase switching, the permeate flow simulated remains almost constant over the cycles due to a permeability defined as a constant as a function of time. This was not the case for the experimental permeate flows. This mismatch became more pronounced when the membrane was subjected to higher transmembrane pressures. As shown in Figure 6a, with an operating 1.2 bar transmembrane pressure, the permeate flow rate dropped from 36.3 $L.h^{-1}$ in the first 5 minutes to 32.7 $L.h^{-1}$ in the last 5 minutes, with a 10% reduction observed in 60 minutes. When the feed pressure was increased to 3.2 bar (inducing a TMP of 2.1 bar) (Fig. 6b), a simulated mean flow rate of 49.5 $L.h^{-1}$ was obtained, compared with an experimental flow rate of 47 $L.h^{-1}$. Between the first 2 minutes of filtration and the last two, the average experimental flow rate fell from 51.6 $L.h^{-1}$ to 46.6 $L.h^{-1}$, i.e. a 10% decrease in 20 minutes. The main reason for this difference is the progressive fouling of the membrane surface, which degrades the permeate flow rate while the transmembrane pressure remains constant. With a transmembrane pressure of 0.9 bar (Fig. 6d),

the impact of fouling was not noticeable over the 20 minutes of experiments, as the flow remained stable at 20.6 $L.h^{-1}$. Fouling was therefore accentuated when transmembrane pressure was high as noted by Crozes et al., 1997 [26].

Although the experiments were carried out with drinking water, provided by the urban distribution network and containing little turbidity and suspended solids, membrane fouling occurred. This issue will be further accentuated when treating surface water [27] and it is, therefore, crucial to consider periodic membrane cleaning to maintain high process performance. The following section is dedicated to the design and evaluation of a backwashing cleaning device, which can be easily integrated into such a thermo-hydraulic filtration process to stabilise its operation and performance.

5. Membrane backwash device

The main drawback of filtration-based water treatment processes lies in the management of membrane fouling. Chemical cleaning, although necessary to remove the irreversibly clogged particles on the surface of the membrane, degrades the membrane life and increases the operating cost [28]. An effective physical cleaning process, such as backwashing, is, therefore, a relevant and an important preventive method against irreversible fouling of membranes, and thus avoids the need for chemical cleaning.

5.1. Design of the backwash device

The backwash device is based on the implementation of a second double-acting cylinder, similar to the hydraulic cylinder used for filtration, into the membrane filtration process (Figure 7). The particularity of this hydraulic cylinder is that it has two chambers of different diameters to allow a pressure-multiplying effect. The driving chamber, located in the upper part of the device, has a larger internal cross-section (S_V = $14.9.10^{-3}$ m^2) than the lower chamber (S_{BW} = $5.67.10^{-3}$ m^2), enabling the pressurisation of the permeate for membrane backwash cleaning. When the cleaning is requested, the membrane feed valve EV_{feed} is closed and the backwash valve EV_{BW} is opened. The upper chamber of the backwash cylinder receives then a flow $\dot{v}_{feed}$ of pressurised water through the main cylinder at P_{feed} pressure. A pair of 3-way solenoid valves direct the piston's movement upwards or downwards, depending on the detection of end-of-stroke switches of this backwash cylinder. Once the piston reaches its end-stop, the switch activates the two 3-way solenoid valves to reverse the direction of the piston movement.

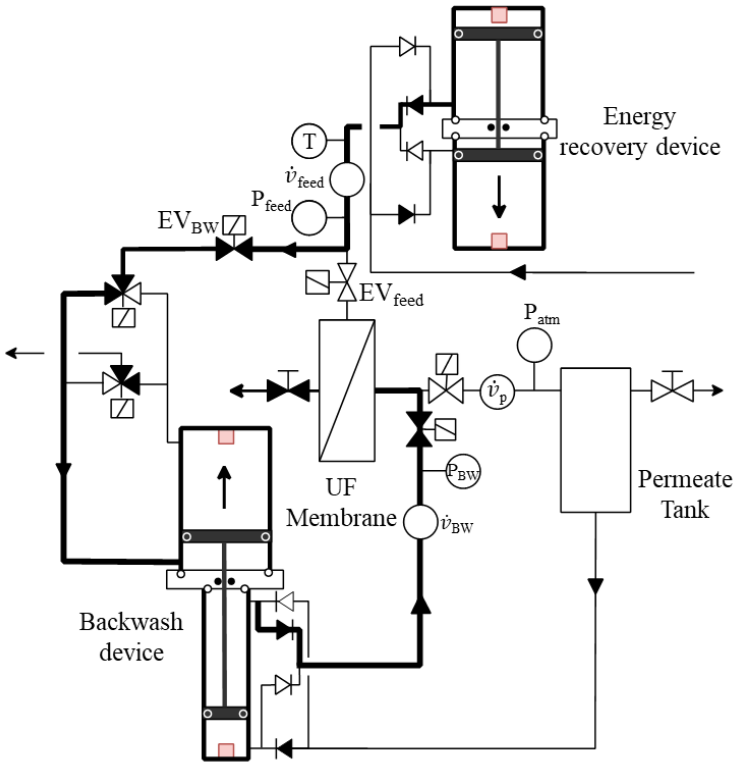

Figure 7. Schematic diagram of the backwash double-acting double-chamber cylinder operation (for clarity, bladder type tanks are not represented).

The hydraulic energy supplied by the larger-diameter piston is transmitted to the smaller-diameter piston in the lower part of the cylinder, enabling it to pump a stream of permeate from the permeate tank, pressurise it and direct it at countercurrent through the membrane module. A set of 4 non-return valves ensures that the permeate is always pumped and pressurised correctly, regardless of the piston's direction of movement.

To facilitate the manufacture of this particular double-acting asymmetric cylinder, the design of its upper chamber is identical (piston section and stroke) to the chambers of the main cylinder. The size of the piston of the lower part is the result of a trade-off between the desired flow rate and the desired pressure of the backwash water. The smaller the diameter of the chamber is, the higher the backwash pressure at the expense of a lower flow rate, and vice versa. As previously established for the main cylinder, the backwash pressure P_{BW} can be similarly estimated (E.14), based on a balance of the driving and resistive forces applied to each side of the piston of the cylinder and by taking into account different pressure losses due to valves which depend on the flow rate. Due to its asymmetric design, the direction of the piston movement is also considered by means of the

Boolean variable (δ), which takes the value 0 when the piston is moving downwards and 1 when the piston is moving upwards.

$$P_{BW} = \frac{\eta_{BW}}{(S_{BW} - (1-\delta)S_s)}[(S_V - (1-\delta)S_s).(P_{feed} - \Delta P_{2V} - \Delta P_{3V})]$$

$$+ \frac{\eta_{BW}}{(S_{BW} - (1-\delta)S_s)}[(S_{BW} - \delta S_s).(P_{atm} - \Delta P_{NR})]$$

$$- \frac{S_V - \delta S_s}{(S_{BW} - (1-\delta)S_s)}(P_{atm} + \Delta P_{3V}) - \Delta P_{NR} - \Delta P_{\dot{v}} \qquad \text{(E.14)}$$

With P_{BW} [Pa] the cylinder output pressure for backwashing, η_{BW} [-] the efficiency of the backwashing cylinder, S_{BW} [m^2] the internal cross-section of the backwashing chamber, ΔP_{2V} [Pa] the pressure losses induced by the 2-way solenoid valve, ΔP_{3V} [Pa] the pressure loss induced by the 3-way solenoid valve, P_{atm} [Pa] the atmospheric pressure, ΔP_{NR} [Pa] the pressure loss induced by the non-return valve, $\Delta P_{\dot{v}}$ [Pa] the pressure loss induced by the flowmeter.

To solve this equation and determine the backwash pressure, one first needs to know the efficiency and the sizing of the pistons of the cylinder, in particular the cross-section of the backwash chamber S_{BW}. An preliminary step for the dimensioning of this chamber was made assuming as the first approximation a realistic efficiency of 0.85. This assumed efficiency, which is of the same order of magnitude as the main cylinder, enable to design in first step the piston sizes of the backwash cylinder by considering an appropriate backwash pressure. The aim is to achieve a backwash pressure P_{BW} that is 1 bar higher than the membrane supply pressure P_{feed}, whatever system operation. Such cleaning conditions would allow effective cleaning of the membrane surface. A piston diameter of the second chamber equal to 80 mm, corresponding to an internal cross-section of the backwash chamber of $S_{BW} = 5.03.10^{-3}$ [m^2] should allow this operating condition to be met over the entire process feed pressure range (2 – 3.5 bar).

5.2. Experimental characterisation of the backwash double-acting cylinder

Once manufactured, the backwashing was characterised to determine its actual hydraulic efficiency. The characterisation results showed an experimental yield lower than expected (Fig. 8) with an average value of 0.74 over the range of feed flow rates studied (20 – 120 $L.h^{-1}$). This low value is explained by a faulty concentricity of the pistons between the upper and lower chambers

of the cylinder, resulting in additional friction. The measurement uncertainties are related to those associated with the machining of the tubes and the piston, the rectification of the internal surfaces (10 µm) and those of pressure sensors (0.05 bar). An experimental correlation of the hydraulic efficiency η_{BW} of the backwashing cylinder was thus obtained (E.15) as a function of the driving feed flow rate $\dot{v}_{feed}$ [L.h^{-1}] ranging from 20 to 120 L.h^{-1}.

$$\eta_{BW} = -1.10^{-4}.\dot{v}_{feed} + 0.746 \qquad \text{(E.15)}$$

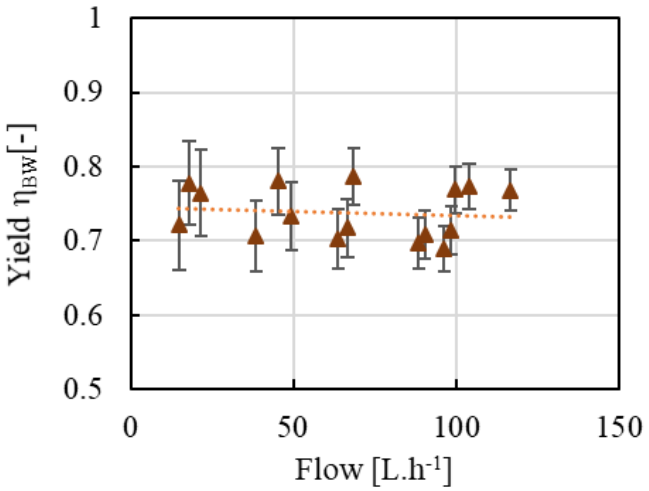

Figure 8. Hydraulic efficiency of the backwashing double–acting cylinder as a function of the flow feed rate in the driving chamber

The ratio of the cross-sections of the two chambers resulted in a lower flow rate of backwashing permeate ($\dot{v}_{BW}$) than that arriving in the driving chamber ($\dot{v}_{feed}$). When the driving flow rate was between 20 and 120 L.h^{-1}, the backwash flow varied between 8 and 50 L.h^{-1}. The backwashing tank was sized to hold a volume of 4.5 L, which allows, under conditions with the highest backwash flow rates (50 L.h^{-1}), the membrane to be cleaned for 5 minutes.

5.3. Experimental study of membrane backwashing

An identical methodology to that applied to the study of the process in dead-end filtration mode was followed for the study of backwashing. Two-experiments are presented in Figure 9. For each of these experiments, the pressures and flow rates upstream (P_{feed}; $\dot{v}_{feed}$) and downstream (P_{BW}; $\dot{v}_{BW}$) of the cylinder were measured. The first one was carried out under high and low pressure operating conditions in the bladder type reservoir of P_{high} = 5.4 bar and P_{low} = 3 bar (Fig. 9a and b) and the second one with P_{high} = 4.5 bar and P_{low} = 3 bar (Fig. 9c and d). For each of these operating conditions, 2.5 backwash cycles, corresponding to two and a half round trips of the

hydraulic cylinder, were carried out in order to control the reproducibility of the backwash cylinder's operation and the effectiveness of the membrane cleaning.

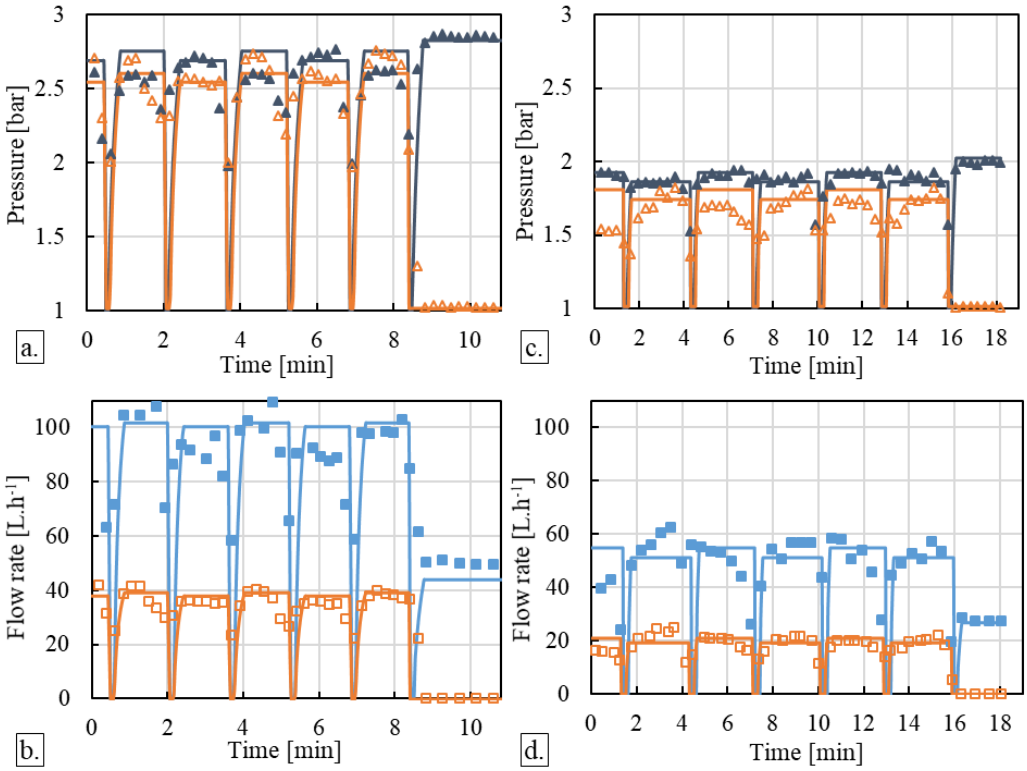

Figure 9. Experimental (dots) and simulated (continuous lines) of feed (full symbols) and backwashing (empty symbols) pressures (▲, △) and flow rates (■, □) produced by the cylinder under high and low operating pressure of respectively (a, b) 5.4 and 3 bar and (c, d) 4.5 and 3 bar.

For both operating conditions, the cycles show a constant periodicity with small fluctuations in the feed rate $\dot{v}_{feed}$. For a feed pressure P_{feed} of 2.6 bar (Fig. 9a), the backwash cycle lasted an average of 3 minutes with an average flow rate $\dot{v}_{feed}$ of 98.2 $L.h^{-1}$ (Fig. 9b) and a pumped permeate flow for backwashing $\dot{v}_{BW}$ of 36.1 $L.h^{-1}$. These backwash cycles were shorter than those obtained for filtration due to higher flow rates $\dot{v}_{feed}$. Piston movement speed remained acceptable, of the order of 1-2 $mm.s^{-1}$. The feed and backwash pressures, however, were of the same order whatever the direction of piston movement. The average pressure P_{feed} over these three cycles was 2.58 bar, compared with 2.54 bar obtained for backwash pressure P_{BW} (Fig. 9a). The efficiency, calculated from the driving and resisting force balances, of the backwash cylinder averaged 0.72 for the three cycles, which was consistent with the previous experimental characterisation of the cylinder (Fig.

8). When the 2.5 backwash cycles are complete, the process switches to filtration mode. Backwash flow rate and pressure respectively reach zero and atmospheric conditions. The feed flow rate $\dot{v}_{feed}$ and therefore permeate flow rate produced by the membrane (dead-end operation) stabilises at 49.8 $L.h^{-1}$ for a transmembrane pressure of 1.8 bar. This reduction in feed flow from 98.2 $L.h^{-1}$ to 49.8 $L.h^{-1}$ allowed a reduction in induced pressure losses in the valves and slightly increased the feed pressure P_{feed} from 2.6 to 2.8 bar.

Figures 9c and 9d show the measured pressures and flow rates obtained for the second experiment when air pressures in the bladder tanks, controlled by the pressure-reducing regulator and the backpressure regulator, were reduced to 4.5 bar and 3 bar respectively. With these conditions, the pressures in the backwashing cylinder were lower than the driving pressure, P_{feed} = 1.87 bar and P_{BW} = 1.65 bar. As a consequence, backwashing was carried out with an average permeate flow rate lower of about 19 $L.h^{-1}$ while backwashing cycles were longer and about 5.5 minutes. After 3 backwash cycles, the device was again switched to filtration mode with a transmembrane pressure of 0.94 bar and an average permeate flow $\dot{v}_p$ of 27.1 $L.h^{-1}$.

For the two detailed experiments, the ratio of the backwash pressure to filtration was between 0.85 to 1.1, lower than the one expected. This does not correspond to the ideal conditions for backwashing operations, but it is not unacceptable and can certainly be improved. To achieve values ranging between 1.5 and 2.5, as recommended in the literature [8], several options are available i.e. (i) change the design of the backwash cylinder, with a smaller cross-section for the backwash chamber to increase the pressure-multiplying effect while reducing the flow rate of pumped permeate and the associated hydraulic losses, (ii) improve concentricity between the two hydraulic chambers to limit the mechanical friction and then increase the hydraulic efficiency, (iii) change the three-way solenoid valves that generate considerable pressure drop due to their small hydraulic cross-section (3 mm) and decrease the pressure level at the inlet of the backwash unit.

Experiments have demonstrated the possibility of carrying out and controlling the filtration and backwashing operation based on two bladder tanks associated with two double chambers. The numerical model previously presented for the process operating in filtration mode was then improved by including the modelling of backwashing by the asymmetric double-acting hydraulic device.

5.4. Modelling of the backwash device

Modelling of the backwash cylinder should enable the backwash flow rate $\dot{v}_{BW}$ and the backwash pressure P_{BW} applied to the membrane to be determined at each time. The backwash flow rate can be determined from the ratio between the cylinder cross-sections and the feed flow $\dot{v}_{feed}$ generated by the main cylinder (E.16).

$$\dot{v}_{BW} = (\dot{v}_{feed}.(S_{BW} - (1-\delta)S_s))/(S_V - (1-\delta)S_s) \quad \text{(E.16)}$$

Backwash pressure results from the balance between the driving and resistant forces applied to the backwash cylinder pistons previously considered for the dimensioning of the cylinder sizing (Eq. 14).

Simulations are shown in Figure 9. Even if the agreement is far from perfect, the general trends are respected for the pressures and the flow rates during the backwashing operation. In Figures 9c and 9d, simulated average pressures are 1.81 bar for the driving pressure P_{feed} and 1.71 bar for the resulting backwash pressure P_{BW} compared to respectively 1.87 bar and 1.65 bar for the experiments. These pressures allowed an average feed flow rate of 48.4 $L.h^{-1}$ (experimental $\dot{v}_{feed}$ = 48.8 $L.h^{-1}$) and a backwash flow rate of 18.3 $L.h^{-1}$ (experimental $\dot{v}_{BW}$ = 18.7 $L.h^{-1}$). The root-mean-square deviation from experimental values was 0.06 bar for pressures and 0.4 $L.h^{-1}$ for flow rates. In the case of the first experiment represented by the graphs in Figures 9a and 9b, the root-mean-square deviation was the same for the pressure with an average of 0.06 bar but higher and equal to 2.27 $L.h^{-1}$ for the flow rates.

5.5. Experiments with river water

Even if not detailed in the dedicated section, in the experiments carried out with the tap water provided by the urban network, the backwashing method effectively cleaned the membrane and, after each backwashing sequence, achieved a permeability equal to or slightly higher than the one specified by the manufacturer (L_0). With tap water, as expected and observed (Fig. 6), fouling is very limited. The effectiveness of the backwashing system was then assessed by performing filtration of raw surface water, taken from a bacterially-charged river located near Perpignan (*La Fossella*, France), 1 km downstream of a wastewater treatment plant. After sampling, it was first pre-filtered using polypropylene filter cartridges with a cut-off of 60 µm and then 20 µm. For these new experiments, sequences of 30 minutes filtration followed by a 3-minute backwash were

carried out. The transmembrane pressure during filtration was 1.47 bar. For the 3-minute backwash, the pressure-reducing regulator setting was manually modified to increase the high pressure P_{high}. The transmembrane pressure during the backwash was then increased to 1.87 bar. Figure 10 shows the evolution of dimensionless membrane permeability referenced by its initial value ($\xi = L/L_0$) over 5 filtration/backwashing sequences.

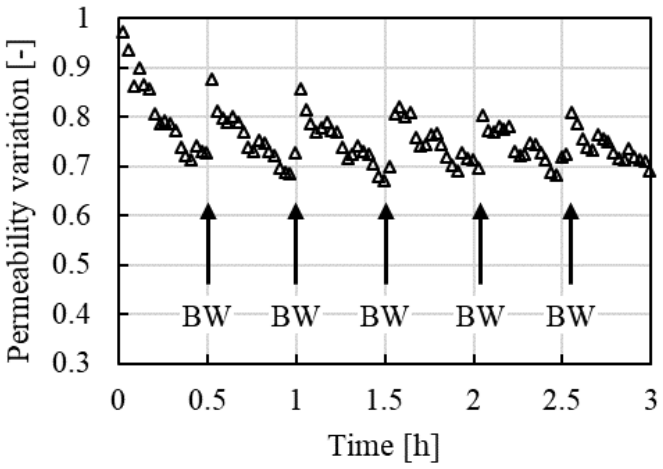

Figure 10. Evolution of the dimensionless membrane permeability during 5 filtration/backwash sequences with bacterially charged raw river water.

During the first thirty-minute filtration sequence, the permeability was reduced by 30% revealing a progressive fouling of the membrane. First backwashing allowed 90% of the initial permeability to be recovered. In the following sequences, the permeability reduction was smaller and appeared to stabilise after the third filtration/backwash sequence. Permeability then varied between 0.8 and 0.7 compared to the initial permeability. Backwashing periodically every thirty minutes therefore makes it possible to maintain and stabilise the filtration performance of the membrane module at acceptable values.

Given the operating conditions, the quasi-steady-state operation of the device is achieved in the experiments by 3 sequences of 30 minutes of filtration and 3 minutes of backwashing. The number of sequences can be higher or lower depending on the quality of the river water. Additionally, the degree of fouling also depends on the membrane operating mode, whether in dead-end or cross-flow mode. As for any membrane filtration process, it will be therefore important to first define the backwashing frequency in relation to the river water quality and to design the components of the thermo-hydraulic process (main cylinder and backwashing cylinder) accordingly, in order to obtain the appropriate backwashing pressure and flow rate for effective membrane cleaning.

6. Conclusion

Ultrafiltration of surface water using solar thermal energy can be an energy efficient disinfection technology for a wide range of microorganisms and pathogens, particularly suited to isolated areas. The innovative thermo-hydraulic membrane filtration process preliminarly descrided in the paper aims to use thermal solar energy at low temperature provided by conventional flat-plate solar collectors, which can provide heat at 40-70°C to power an engine Organic Rankine - like Cycle in order to produce hydraulic pressure energy. The hydraulic pressure energy produced is then used by various hydraulic devices to pump, pressurise and filter safely raw water, and to backwash the ultrafiltration module. The work presented in this article is a first step towards the development of such a process, focusing more particularly on the study of the hydraulic part of the filtration and backwashing process.

In this preliminary feasibility study, the operating high pressure of the UF process, that will be imposed in a second step by the evaporator of the ORC cycle, is achieved using a pressure-reducing regulator fed by an air compressor. The operating low pressure that will be imposed by the condenser of the ORC cycle is achieved by a controlled open-air discharge from a backpressure regulator.

Pressures and flow rates at different points of the process were analysed for different high and low pressures (P_{high}, P_{low}), representative of the evaporator and condenser operating conditions of a solar ORC using butane as the working fluid. These conditions varied over a wide range of pressures, from 3 to 6.5 bar for the high pressure and from 1.5 to 4 bar for the low pressure, corresponding respectively to an evaporation temperature varying from 35 to 65°C and a condensation temperature varying from 10 to 40°C. In every case, air pressure energy transmitted via bladder-type tanks pressurises a transfer liquid driving a main cylinder. It has been demonstrated experimentally that, whatever the operating conditions, this double-chamber, double-acting cylinder can in turn pump, pressurise and filter raw surface water through a UF module with an efficiency of around 90%. This main cylinder also enables a second cylinder to be operated, which ensures a periodic physical cleaning of the UF membrane module by pumping a small amount of permeate produced and pressurising it to backwash the membrane with yields of the order of 75%. The experiments showed reproducible process behaviour with filtration cycles ranging from 6 to 13 minutes, depending on the pressure conditions applied.

Simulations carried out using dynamic modelling of the process showed a high degree of agreement with the experiments undertaken. Average deviations of 6.4% on flow rates and 1.6% on pressures were observed with the simulation results for all experiments.

Backwashing is an integral part of any membrane filtration process. Without backwashing and as expected, filtration of raw river water leads to significant clogging mechanisms and as a consequence, degradation of the membrane performance. It is therefore important to define the backwashing operating conditions i.e. appropriate backwashing pressure and flow rate, frequency and duration, in relation to the water quality to be filtered. A stabilisation of the membrane permeability between 70 and 80% of its initial value (L_0) has been achieved by performing 30-minute filtration sequences at a transmembrane pressure of 1.5 bar followed by a 3-minute backwashing at a TMP of 1.9 bar. During backwashing and because of the discussed low hydraulic efficiency of the backwashing cylinder, the high pressure was increased to be able to reach such a TMP value. Anyway, the tests carried out have validated the global concept of backwashing with a second double-acting asymmetric cylinder. More generally, they opened the way to the design of a thermo-hydraulic ultrafiltration process powered by low temperature thermal energy.

This preliminary study aimed to assess the behaviour and characterise the hydraulic components of the planned solar thermo-hydraulic process, performing the pumping and filtration of surface water and the backwashing of the membrane. The next step of this work will focus on the integration of the engine Organic Rankine Cycle coupled with a flat-plate solar collector. The objective of the second part of this development study will be to experiment and analyse the operation of the complete thermo-hydraulic process, with the ORC cycle coupled to the hydraulic part studied in this work, in order to characterise its energy performance according to evaporation and condensation temperatures.

Corresponding Author

Corentin Koninck – Process, Materials and Solar Energy (PROMES) - Université de Perpignan Via Dominitia (UPVD), 500 Rambla de la Thermodynamique, 66100 Perpignan, France; https://orcid.org/0009-0008-3988-2860; E-mail: corentin.koninck@promes.cnrs.fr

Author Contributions

The manuscript was written through contributions of all authors. All authors have given approval for the final version of the manuscript. The authors declare no competing financial interest.

Supporting information

This work is accompanied by an additional appendix section with 3 parts:

- Part S1: Characteristic data of components and sensors (docx)
- Part S2: LabVIEW interface and experimental results (docx)
- Part S3: Detail of the calculation of the equations describing the membrane filtration model (docx)
- Part S4: Variables used in the membrane filtration model (docx)

Funding Sources

This study was supported by the Region Occitanie for PhD grant, the French Government through the “Investissements d’avenir” (Investment for the Future) program of the Agence Nationale de la Recherche (National Agency for Research) under award number ANR-10-LABX-22-01-SOLSTICE. This work also received European support from the European Union's Horizon2020 Research and Innovation programme SFERA-III under grant agreement n°823802.

REFERENCES

[1] Prüss-Ustün, A., Wolf, J., Bartram, J., Clasen, T., Cumming, O., Freeman, M.C., Gordon, B., Hunter, P.R., Medlicott, K., Johnston, R., Burden of disease from inadequate water, sanitation and hygiene for selected adverse health outcomes: An updated analysis with a focus on low- and middle-income countries. International Journal of Hygiene and Environmental Health, **2019**, 222, 765–777. DOI: 10.1016/j.ijheh.2019.05.004

[2] WHO, UNICEF, World Bank., State of the world's drinking water: an urgent call to action to accelerate progress on ensuring safe drinking water for all. Geneva: World Health Organization. **2022**.

[3] Othman, N.H., Alias, N.H., Fuzil, N.S., Marpani, F., Shahruddin, M.Z., Chew, C.M., David Ng, K.M., Lau, W.J., Ismail, A.F., A Review on the Use of Membrane Technology Systems in Developing Countries. Membranes (Basel), **2021**, 12, 30. DOI: 10.3390/membranes12010030

[4] Hoslett, J., Massara, T.M., Malamis, S., Ahmad, D., van den Boogaert, I., Katsou, E., Ahmad, B., Ghazal, H., Simons, S., Wrobel, L., Jouhara, H., Surface water filtration using granular media and membranes: A review. Science of The Total Environment, **2018**, 639, 1268–1282. DOI: 10.1016/j.scitotenv.2018.05.247

[5] Glucina, K., Laîne, J.M., Durand-Bourlier, L., Assessment of filtration mode for the ultrafiltration membrane process. Desalination, Conference Membranes in Drinking and Industrial Water Production, **1998**, 118, 205–211. DOI: 10.1016/S0011-9164(98)00131-3

[6] Peter-Varbanets, M., Zurbrügg, C., Swartz, C., Pronk, W., Decentralized systems for potable water and the potential of membrane technology. Water Research, **2009**, 43, 245–265. DOI: 10.1016/j.watres.2008.10.030

[7] Doyen, W., Baée, B., Beeusaert, L., UF as an alternative pretreatment step for producing drinking water. Membrane Technology, **2000**, 2000, 8–13. DOI: 10.1016/S0958-2118(00)80235-9

[8] Jacangelo, J.G., Rhodes Trussell, R., Watson, M., Role of membrane technology in drinking water treatment in the United States. Desalination, Workshop on Membranes in Drinking Water Production Technical Innovations and Health Aspects, **1997**, 113, 119–127. DOI: 10.1016/S0011-9164(97)00120-3

[9] Van Der Bruggen, B., Vandecasteele, C., Van Gestel, T., Doyen, W., Leysen, R., A review of pressure-driven membrane processes in wastewater treatment and drinking water production. Environmental Progress, **2003**, 22, 46–56. DOI: 10.1002/ep.670220116

[10] Crittenden, J.C., Rhodes Trussell, R., Hand, D.W., Howe, K.J., Tchobanoglous, G., Membrane Filtration, in: MWH's Water Treatment: Principles and Design, **2012**, Third Edition. John Wiley & Sons, Ltd, pp. 819–902. DOI: 10.1002/9781118131473.ch12

[11] Pearce, G.K., UF/MF pre-treatment to RO in seawater and wastewater reuse applications: a comparison of energy costs. Desalination, European Desalination Society and Center for Research and Technology Hellas (CERTH), **2008**, Halkidiki, Greece 222, 66–73. DOI: 10.1016/j.desal.2007.05.029

[12] Pronk, W., Ding, A., Morgenroth, E., Derlon, N., Desmond, P., Burkhardt, M., Wu, B., Fane, A.G., Gravity-driven membrane filtration for water and wastewater treatment: A review. Water Research, **2019**, 149, 553–565. DOI : 10.1016/j.watres.2018.11.062

[13] Fonto de Vivo, *ORISA® - la filtration d'eau humanitaire pour les ONG et associations. FONTO DE VIVO*, 2021, URL https://www.fontodevivo.fr/filtration-deau-humanitaire/ (accessed 4.9.24).

[14] Arnal, J.M., Sancho Fernández, M., Martín Verdú, G., Lora García, J., Design of a membrane facility for water potabilization and its application to Third World countries. Desalination, **2001**, 137, 63–69. DOI: 10.1016/S0011-9164(01)00205-3

[15] Hoffman, A.R., Water Security: A Growing Cris is and the Link to Energy. AIP Conference Proceedings, **2008**, 1044, 55–63. DOI: 10.1063/1.2993738

[16] Michael, J.J., Selvarasan, I., Economic analysis and environmental impact of flat plate roof mounted solar energy systems. Solar Energy, **2017**, 142, 159–170. DOI: 10.1016/j.solener.2016.12.019

[17] Davey, J., Schäfer, A.I., Ultrafiltration to Supply Drinking Water in International Development: A Review of Opportunities, in: Yanful, E.K. (Ed.), Appropriate Technologies for Environmental Protection in the Developing World: Selected Papers from ERTEP 2007, July 17–19 2007, Ghana, Africa. Springer Netherlands, Dordrecht, **2009**, pp. 151–168. DOI: 10.1007/978-1-4020-9139-1_16

[18] Czarny, J., Präbst, A., Spinnler, M., Biek, K., Sattelmayer, T., Development and Simulation of Decentralised Water and Energy Supply Concepts – Case Study of Rainwater Harvesting at the Angkor Centre for Conservation of Biodiversity in Cambodia, J. sustain. dev. energy water environ. syst., **2017**, 5(4), pp 626-644. DOI: 10.13044/j.sdewes.d5.0171

[19] Baú, S.R.C., Bevegnu, M., Giubel, G., Gamba, V., Cadore, J.S., Brião, V.B., Shaheed, M.H., Development and economic viability analysis of photovoltaic (PV) energy powered decentralized ultrafiltration of rainwater for potable use. Journal of Water Process Engineering, **2022**, 50, 103228. DOI: 10.1016/j.jwpe.2022.103228

[20] Chew, C.M., David Ng, K.M., Feasibility of solar-powered ultrafiltration membrane water treatment systems for rural water supply in Malaysia. Water Supply, **2019**, 19, 1758–1766. DOI: 10.2166/ws.2019.050

[21] Alharbi, F.H., Kais, S., Theoretical limits of photovoltaics efficiency and possible improvements by intuitive approaches learned from photosynthesis and quantum coherence. Renewable and Sustainable Energy Reviews, **2015**, 43, 1073–1089. DOI: 10.1016/j.rser.2014.11.101

[22] Venkateswari, R., Sreejith, S., Factors influencing the efficiency of photovoltaic system. Renewable and Sustainable Energy Reviews, **2019**, 101, 376–394. DOI: 10.1016/j.rser.2018.11.012

[23] Lacroix, C., Perier-Muzet, M., Stitou, D., Dynamic Modeling and Preliminary Performance Analysis of a New Solar Thermal Reverse Osmosis Desalination Process. Energies, **2019**, 12, 4015. DOI: 10.3390/en12204015

[24] Huisman, I.H., Dutré, B., Persson, K.M., Trägårdh, G., Water permeability in ultrafiltration and microfiltration: Viscous and electroviscous effects. Desalination, **1997**, 113, 95–103. DOI: 10.1016/S0011-9164(97)00118-5

[25] Tarnawski, V.R., Jelen, P., Estimation of compaction and fouling effects during membrane processing of cottage cheese whey. Journal of Food Engineering, **1986**, 5, 75–90. DOI: 10.1016/0260-8774(86)90020-8

[26] Crozes, G.F., Jacangelo, J.G., Anselme, C., Laîné, J.M., Impact of ultrafiltration operating conditions on membrane irreversible fouling. Journal of Membrane Science, **1997**, 124, 63–76. DOI: 10.1016/S0376-7388(96)00244-X

[27] Huang, H., Lee, N., Young, T., Gary, A., Lozier, J.C., Jacangelo, J.G., Natural organic matter fouling of low-pressure, hollow-fiber membranes: Effects of NOM source and hydrodynamic conditions. Water Research, Membranes, **2007**, 41, 3823–3832. DOI: j.watres.2007.05.036

[28] Chang, H., Liang, H., Qu, F., Liu, B., Yu, H., Du, X., Li, G., Snyder, S.A., Hydraulic backwashing for low-pressure membranes in drinking water treatment: A review. Journal of Membrane Science, **2017**, 540, 362–380. DOI: 10.1016/j.memsci.2017.06.077